Korean Journal of Nuclear Medicine Technology, Volume 30, Number 1, Article 8, May 2026.
Korean J Nucl Med Technol 2026;30(1):8. https://doi.org/10.12972/kjnmt.2026.30.1.8
pISSN 1229-9901
eISSN 2982-8406

Original article

핵의학 영상 검사에서 베개 높이 표준화를 위한 연구: 병변 왜곡 중심

김태헌, 방사선사, 류재광*, 방사선사, 김한울, 방사선사, 정우영, 방사선사
서울아산병원 핵의학과

Standardization of Pillow Height in Nuclear Medicine Imaging: Focus on Lesion Distortion

Tae-Heon Kim, Radiological Technologist, Jae-Kwang Ryu*, Radiological Technologist, Han-Ul Kim, Radiological Technologist, Woo-Young Jung, Radiological Technologist
Department of Nuclear Medicine, Asan Medical Center, Seoul, Korea

***Corresponding Author: Jae-Kwang Ryu.** Department of Nuclear Medicine, Asan Medical Center, Seoul, Korea, 88, Olympic-ro 43-gil, Songpa-gu, Seoul, 05505, Republic of Korea. Tel: +82-2-3010-5421, E-mail: huhjoon11@naver.com

ABSTRACT

Purpose: Due to the lack of standardized manufacturer guidelines for pillow height in nuclear medicine, clinical practices often rely on empirical experience. This study evaluates the effect of head elevation on image quality and lesion distortion using an ACR (American College of Radiology) phantom to establish the optimal standardized height for maintaining diagnostic accuracy. **Materials and Methods**: Images were acquired using a Siemens Symbia E gamma camera equipped with a LEHR (Low-Energy High-Resolution) collimator. To simulate intracranial lesions, the hot cylinders of an ACR phantom(25, 16, 12, and 8 mm) were utilized with a target to background radioactivity ratio of 10:1. The phantom was elevated from the table in 2 cm increments (0, 2, 4, and 6 cm, with 5-minute static images acquired at each height. Quantitative analysis of total counts, length, area, and FWHM (full width at half maximum) was performed under three ROI (Region of Interest) conditions: (1) Auto ROI with an 80% threshold, (2) Fixed-size ROI, and (3) Modified ROI defined by isolating the high-intensity red spectrum within a Rainbow color scale. All results were expressed as percentage reductions relative to the baseline values at 0 cm. **Results**: Three analytical parameters (total counts, area, and length) exhibited a downward trend as height increased from the 0 cm baseline, while the FWHM demonstrated a corresponding upward trend. In the Auto ROI analysis, total counts at 6 cm decreased by 26% (8 mm), 34.4% (12 mm), and 14% (16 mm and 25 mm) compared to 0 cm. The most rapid decline in counts occurred at different intervals depending on cylinders size: 0–2 cm for the 8 mm lesion, 2–4 cm for the 12 mm lesion, and 4–6 cm for both 16 mm and 25 mm lesions. Furthermore, compared to the baseline at 0 cm, the FWHM values at a height of 6 cm increased by 24.9% for the 8 mm cylinder, 24.2% for the 12 mm cylinder, 14.7% for the 16 mm cylinder, and 10.1% for the 25 mm cylinder. **Conclusion**: Head elevation significantly induces lesion distortion and degrades image quality, with small lesions (≤12 mm) exhibiting higher sensitivity to minor distance changes. While larger lesions show prominent distortion beyond 2 cm, smaller lesions are affected immediately. To minimize diagnostic inaccuracy, it is recommended that the height of the pillow or headgear be maintained below 2 cm and must not exceed 4 cm.

Keywords: Pillow Height, Distortion, FWHM, ACR Phantom

Received April 10, 2026 **Revised** April 25, 2026 **Accepted** April 28, 2026

Introduction

The skeletal system is the most frequent site of metastasis for solid tumors, particularly in breast and prostate cancers. Given the high prevalence of bone metastasis in specific malignancies, continuous monitoring of skeletal involvement and early intervention are critical components in the treatment of high-risk cancer patients[1]. The primary principle of bone scintigraphy is the precise localization of lesions. Achieving this requires optimization of the examination process to acquire high-quality images and provide the most clinically useful diagnostic information[2]. However, bone scans are frequently performed on different dates, using various equipment, protocols, and facilities, and by different technologists; furthermore, operational data for each scan may be inconsistent or inaccessible. Maintaining identical anatomical geometry across multiple scans is challenging due to variables such as patient positioning, the curvature of the spine and neck, limb placement, table configuration, respiratory status, cardiac cycle, and gastrointestinal or urinary conditions all of which can compromise diagnostic accuracy[3]. Prior research has demonstrated that the use of pillows combined with Chang's attenuation correction can significantly influence cerebral blood flow values in the anterior and posterior regions of the brain[4]. Subsequent studies have investigated pillow materials that minimize radiation attenuation[5]. Nevertheless, to date, no study has simultaneously evaluated the combined impact of attenuation correction methods and the presence or absence of a pillow. In nuclear medicine imaging, the detectability and quantitative accuracy of lesions are determined by physical factors such as spatial resolution, total counts, T/B (target to background) ratio, and FWHM (full width at half maximum)[6]. Specifically, in head imaging, an increase in the height of the patient's head reduces the source-to-detector distance in the anterior view while increasing it in the posterior view. This variation induces changes in geometric blurring and spatial resolution[7,8]. Consequently, lesion boundaries become indistinct, and the radioactive signal that should be concentrated within the lesion disperses into surrounding tissues[2]. This results in a reduction in maximum and total counts, as well as a decrease in the T/B ratio[9]. Thus, changes in head height represent more than a simple postural difference; they directly affect key physical parameters of nuclear medicine images, potentially serving as critical variables in lesion detection sensitivity and quantitative accuracy. Therefore, this study aims to quantitatively analyze lesion distortion according to pillow height using an ACR phantom and to propose an optimal standardized pillow height to minimize such distortion.

Materials and Methods

1. Instrumentation and Phantom

A dual-head gamma camera system (Symbia E, Siemens, Germany) equipped with LEHR(Low-Energy High-Resolution) collimators was employed for data acquisition (Fig. 1). For image quality evaluation and quantitative analysis, the ACR (American College of Radiology) PET (Positron Emission Tomography) Hot Cylinder Phantom was utilized (Fig. 2).

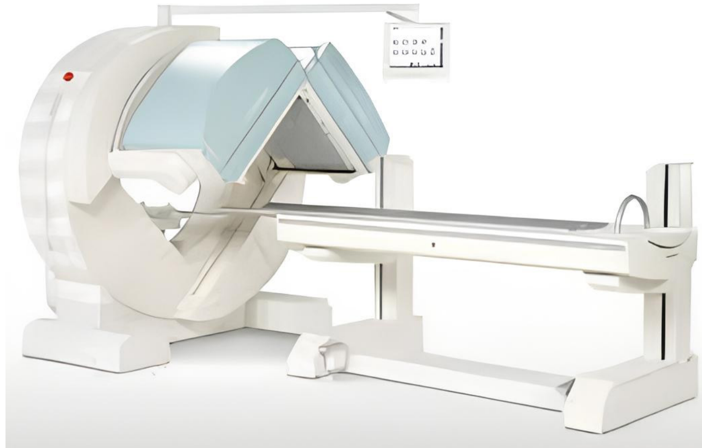

Fig. 1. Dual-head gamma camera with LEHR Collimator was used for image acquisition(Symbia E, Siemens, Germany).

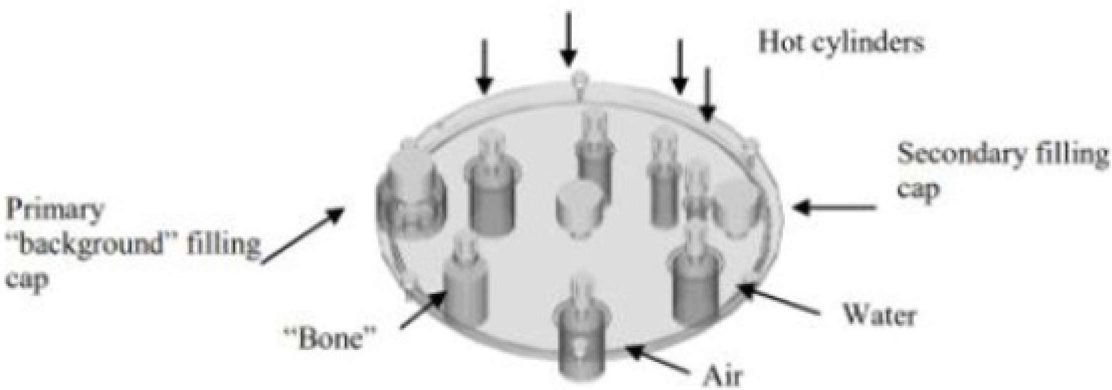

Fig. 2. It is a schematic diagram of PET Phantom viewed from above.

2. Experimental Procedures

To simulate intracranial lesions, four hot cylinders of different volumes (diameters: 25, 16, 12, and 8 mm) within an ACR phantom were utilized. The target-to-background radioactivity ratio was established at 10:1. A preliminary random survey of 20 clinical pillows and headrests (10 polyurethane foam and 10 memory foam) identified 2 cm, 4 cm, and 6 cm as the most frequent heights (Fig. 3, Table 1). The linear attenuation coefficients, densities, and quantities of the pillows, headrests, and the Styrofoam used in the experiment are summarized (Table 2). Styrofoam was selected as the elevation medium because its air-equivalent properties minimize the impact of attenuation and scattering. While minor differences in attenuation exist between the materials, they are negligible compared to soft tissue. Therefore, to maintain physical objectivity and ensure clinical relevance, the SDD (source to detector distance) was strictly controlled in correlation with the phantom elevation. The phantom was elevated in 2 cm increments using Styrofoam boards; each 2 cm increase in height corresponded to a 2 cm reduction in the SDD for the anterior view, which directly modifies the geometric efficiency between the source and the detector. This setup allowed for a quantitative evaluation of geometric resolution and distortion as a function of physical distance (Fig. 4). To ensure clinical validity, the real-time count rate monitored on the system was set to 2.0 kcnts/sec, reflecting the typical values observed during the cranial phase of a clinical bone scan. Image acquisition was performed under standard clinical protocol conditions (Table 3), referencing the SNMMI Procedure Standard for Bone Scintigraphy 4.0. Five-minute static images were acquired at each height in the anterior projection.

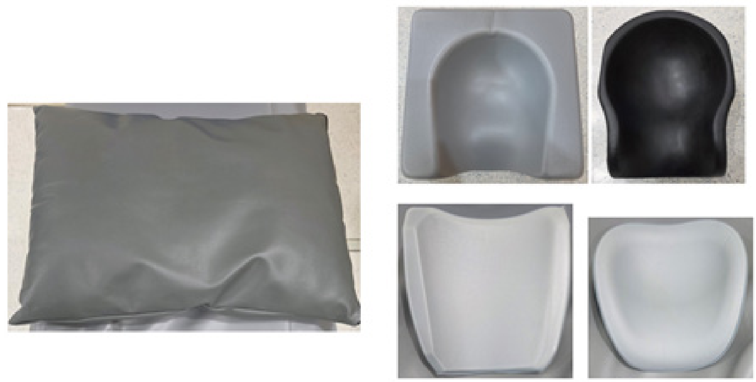

(A) (B)

Fig. 3. (A) Memory foam pillow used in the experiment. (B) Polyurethane foam headrest used in the experiment.

Table 1. Height analysis of 20 clinical pillows and headrests

Pillow height(cm)	Physical SDD(Anterior, cm)	Quantity
0	d	
1	d-1	2
2	d-2	8
3	d-3	1
4	d-4	4
5	d-5	2
6	d-6	3

Table 2. Physical Properties and Attenuation Characteristics of Materials

Material	Linear Attenuation Coefficient(μ, cm^{-1})	Density(g/cm^3)	Quantity
Polyurethane Foam	0.004-0.010	0.03-0.07	10
Memory Foam	0.007-0.018	0.05-0.12	10
Styrofoam	0.003-0.007	0.02-0.05	-

Table 3. Acquisition Parameters of Bone Scan

	Bone Scan
Energy peak & window	15% window centered at 140 keV
Zoom factor	1.23
Matrix	256*256
Time per view	5 min
View	[ANT]

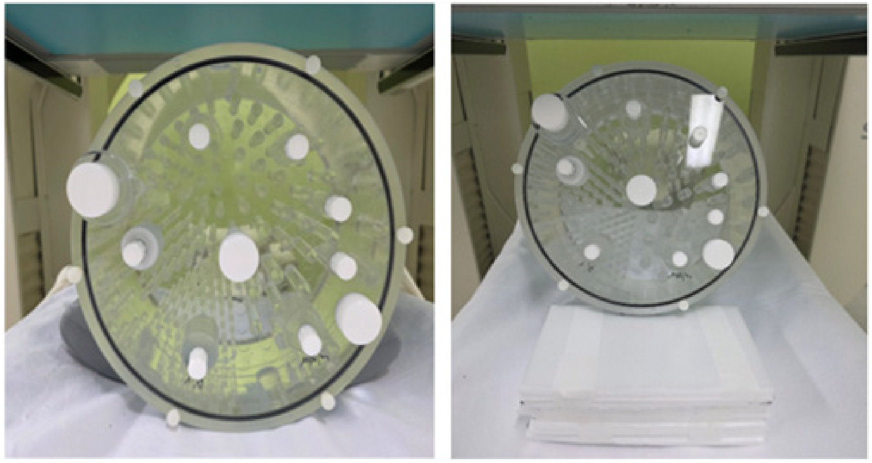

(A) (B)

Fig. 4. Representative images of the ACR phantom used in the experiment. (A) Baseline image acquired at 0 ㎝(table level). (B) Image acquired with the phantom elevated to 6 ㎝ using foam blocks.

3. Data Analysis

The acquired images were analyzed using the following three methods.

3. 1. Auto ROI Analysis

To minimize the potential for observer bias inherent in manual analysis, an automated ROI (Region of Interest) method was employed using the Series ROI Curve Generic Processing feature provided by the Siemens system. The threshold was set at 80%, automatically defining the ROI to include only pixels within this intensity range. For each of the four phantom heights (0 cm, 2 cm, 4 cm, and 6 cm), the total counts, area, FWHM, and length were measured within the defined ROIs (Fig. 5).

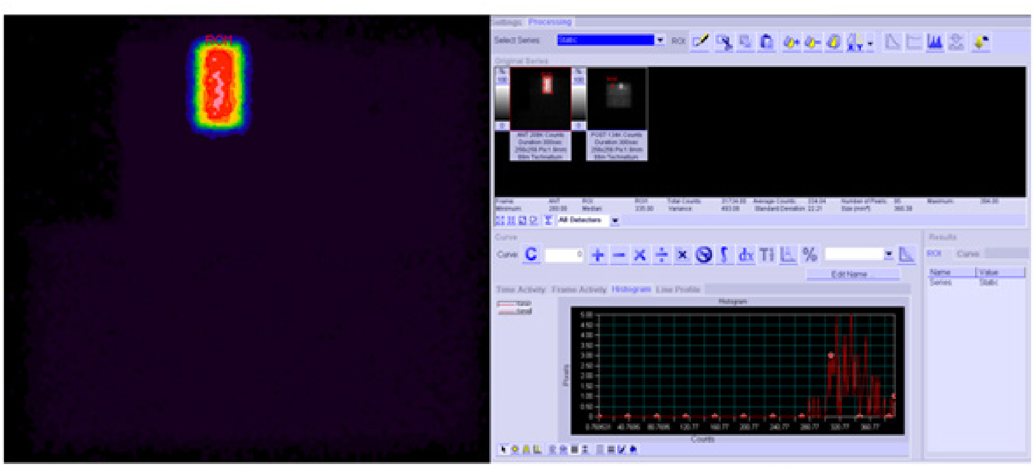

(A) (B)

Fig. 5. (A) The procedure for Auto ROI setup is illustrated. (B) The ROI analysis results are presented.

3. 2. Modified ROI Analysis

To further mitigate the subjectivity associated with manual segmentation, the image color scale was converted to a Rainbow 10-step palette using the Series ROI Curve Generic Processing function on the Siemens workstation. Subsequently, ROIs were defined by isolating only the areas corresponding to the dark red spectrum, which represents the highest pixel intensities. For each of the four phantom heights (0 cm, 2 cm, 4 cm, and 6 cm), the total counts, area, FWHM, and length were quantitatively measured (Fig. 6).

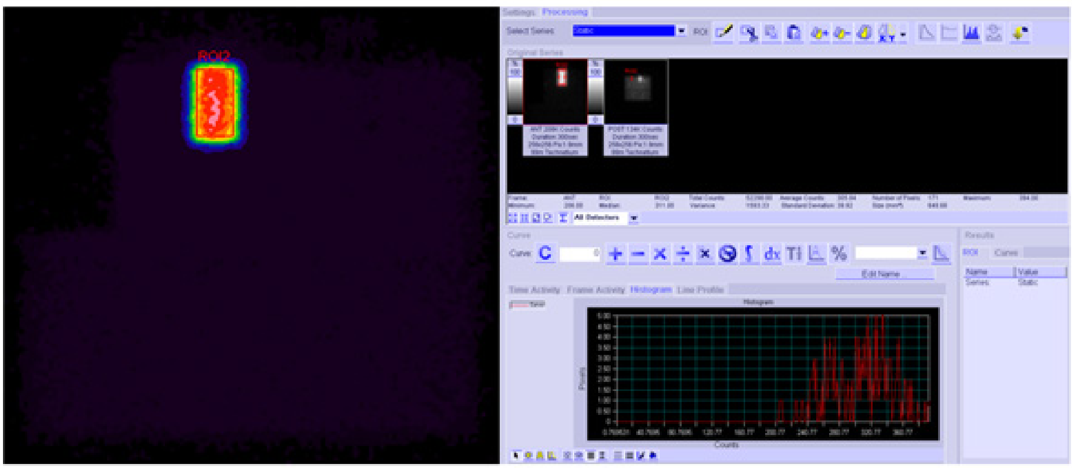

(A) (B)

Fig. 6. (A) The procedure for Modified ROI setup is illustrated. (B) The ROI analysis results are presented.

3. 3. Fixed ROI Analysis

To further minimize the potential for inter-observer variability, a standardized rectangular ROI with a fixed dimension of 14×20 pixels was established using the Series ROI Curve Generic Processing function. This specific size was determined based on the area encompassing the dark red spectrum of the smallest lesion (8 mm diameter). This fixed ROI was applied consistently across all acquired images to ensure comparative accuracy. For each of the four phantom heights (0 cm, 2 cm, 4 cm, and 6 cm), the total counts, area, FWHM, and length were measured(Fig. 7).

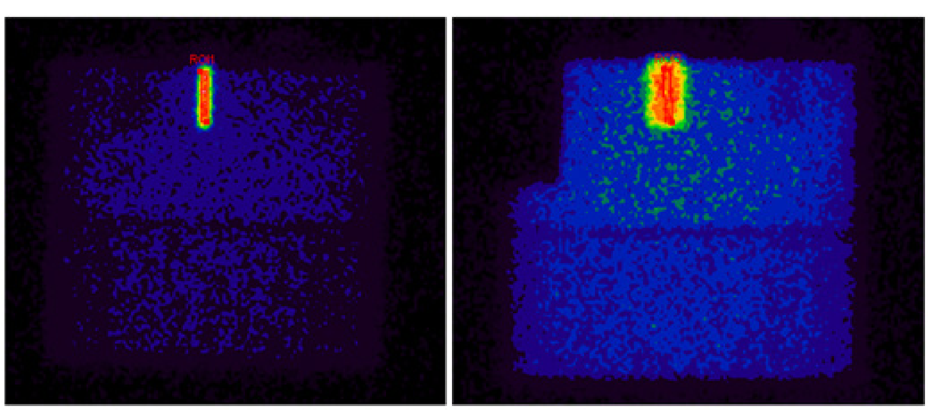

(A) (B)

Fig. 7. (A) The procedure for Fixed ROI setup is illustrated. (B) Representative image of Region of Interest (ROI) placement on a 26 mm lesion using an 8 mm fixed-size ROI.

Results

Using the three ROI analysis methods described above, we analyzed the total counts, area, FWHM, and length measured from the images acquired at four different heights (0 cm, 2 cm, 4 cm, and 6 cm).

1. Total Counts

1.1. Auto ROI Analysis

In the Auto ROI analysis, the total counts generally exhibited a downward trend as the height increased. Compared to the baseline 0 cm, the total counts at a height of 6 cm decreased by 26% for the smallest lesion (8 mm) and by 34.4% for the 12 mm lesion. Both the 16 mm and 25 mm lesions showed a 14% reduction in total counts. An analysis of the rate of change per distance interval revealed that the intervals showing the most rapid decline varied depending on the lesion size. For the 8 mm small lesion, the most significant decrease in counts was observed in the initial interval between 0 cm and 2 cm. For the 12 mm lesion, the most rapid decline occurred between 2 cm and 4 cm, while the 16 mm and 25 mm lesions exhibited their sharpest reductions in the 4 cm to 6 cm interval (Table 4).

Table 4. Quantitative analysis of total counts, percentage changes from 0 cm and step changes in Auto ROI according to elevation height

Diameter (mm)	Distance(cm)	Total Counts	Change from 0 cm (%)	Step Change(%)
25	0	35624	-	-
	2	34052	-4.4	-4.4
	4	32500	-8.9	-4.5
	6	30842	-14.0	-5.1
16	0	14550	-	-
	2	14162	-2.7	-2.7
	4	13482	-7.5	-4.8
	6	12665	-14.0	-6.1
12	0	9362	-	-
	2	9039	-3.5	-3.5
	4	7859	-16.6	-13.1
	6	6660	-34.4	-15.3
8	0	4489	-	-
	2	4121	-8.2	-8.2
	4	3788	-17.0	-8.1
	6	3503	-26.0	-7.5

1.2. Modified ROI Analysis

In the Modified ROI analysis, the total counts generally demonstrated a consistent decline as the distance increased. Compared to the baseline 0 cm, the total counts at a height of 6 cm decreased by 18.2% for the smallest lesion (8 mm) and by 22.7% for the 12 mm lesion. Significant reductions were also observed for the 16 mm and 25 mm lesions, which showed decreases of 31.6% and 16%, respectively. The analysis of change per distance interval revealed that for the 8 mm small lesion and the 12 mm lesion, the most rapid decline in counts occurred in the initial interval between 0 cm and 2 cm. In contrast, for the larger 16 mm and 25 mm lesions, the most significant reduction in counts was observed in the 4 cm to 6 cm interval (Table 5).

Table 5. Quantitative analysis of total counts, percentage changes from 0 cm and step changes in Modified ROI according to elevation height

Diameter (mm)	Distance(cm)	Total Counts	Change from 0 cm (%)	Step Change(%)
25	0	58398	-	-
	2	55824	-4.4	-4.4
	4	53258	-9.2	-4.6
	6	48250	-16.0	-9.4
16	0	22359	-	-
	2	20506	-8.3	-8.3
	4	18724	-17.7	-8.7
	6	16448	-31.6	-12.2
12	0	15547	-	-
	2	13411	-13.7	-13.7
	4	12554	-19.3	-6.4
	6	12011	-22.7	-4.3
8	0	7012	-	-
	2	6506	-7.2	-7.2
	4	6081	-13.3	-6.5
	6	5736	-18.2	-5.7

1.3. Fixed ROI Analysis

In the Fixed ROI analysis, the total counts also exhibited an overall downward trend as the distance increased. Compared to the baseline 0 cm, the total counts at a height of 6 cm decreased by 5.3% for the smallest lesion (8 mm) and by 7.3% for the 12 mm lesion. For the 16 mm and 25 mm lesions, the reductions were 6.3% and 6.4%, respectively. The analysis of change per distance interval revealed that the intervals of most rapid decline varied according to lesion size. For the 8 mm small lesion, the most significant count reduction occurred in the initial interval between 0 cm and 2 cm. For the 12 mm lesion, the most rapid decline was observed between 2 cm and 4 cm, while for the larger 16 mm and 25 mm lesions, the sharpest decreases were recorded in the 4 cm to 6 cm interval (Table 6).

Table 6. Quantitative analysis of total counts, percentage changes from 0 cm and step changes in Fixed ROI according to elevation height

Diameter (mm)	Distance(cm)	Total Counts	Change from 0 cm (%)	Step Change(%)
25	0	25474	-	-
	2	25080	-1.5	-1.5
	4	24776	-2.7	-1.2
	6	23852	-6.4	-3.7
16	0	15021	-	-
	2	14968	-0.4	-0.4
	4	14697	-2.2	-1.8
	6	14069	-6.3	-4.3
12	0	11123	-	-
	2	11040	-0.7	-0.7
	4	10550	-5.2	-4.4
	6	10312	-7.3	-2.3
8	0	6595	-	-
	2	6435	-2.4	-2.4
	4	6337	-3.9	-1.5
	6	6247	-5.3	-1.4

The following graphs provide a comprehensive overview of the total counts and the percentage change relative to the 0 cm baseline for the four lesion sizes across the three ROI analysis methods (Fig. 8, 9).

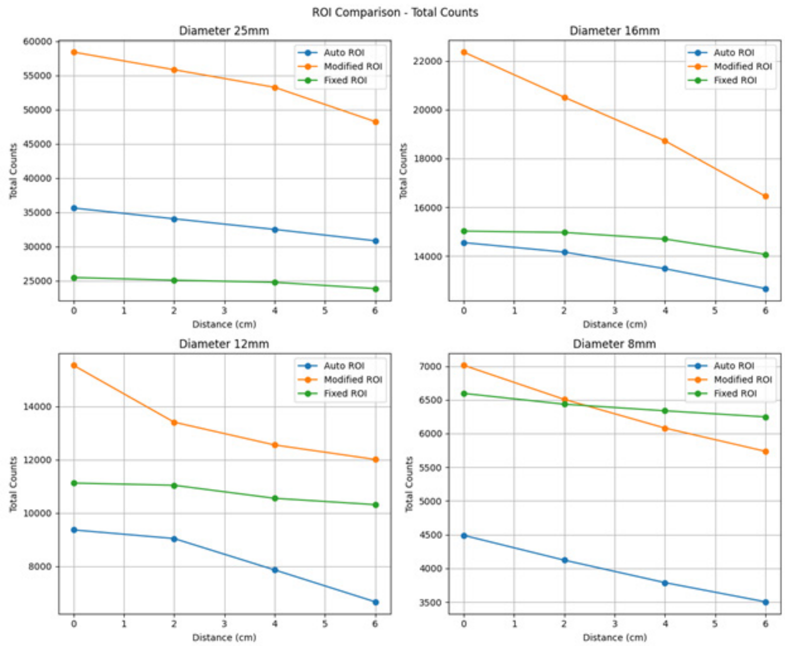

Fig. 8. This figure illustrates the comparison of total count analysis using three different ROI methods: Auto ROI, Modified ROI, and Fixed ROI.

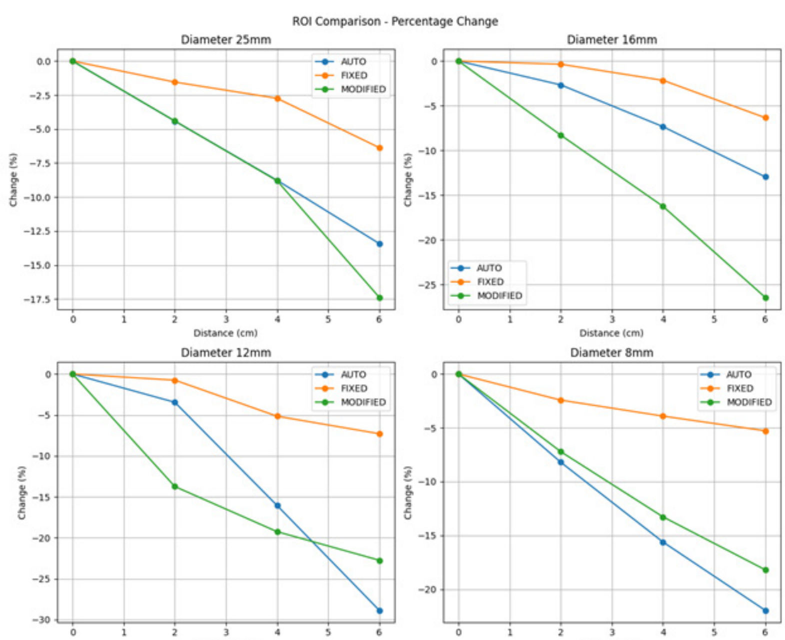

Fig. 9. This figure illustrates the comparison of total count percentage changes from 0 cm analysis using three different ROI methods: Auto ROI, Modified ROI, and Fixed ROI.

2. Area

2.1. Auto ROI Analysis

In the Auto ROI analysis, the area of the smallest lesion (8 mm) decreased by 16.3% at a height of 6 cm compared to the baseline 0 cm, while the area of the 12 mm lesion showed a significant reduction of 34%. For the 16 mm and 25 mm lesions, the area decreased by 16.2% and 13.9%, respectively. The analysis of change per distance interval revealed that for the 8 mm small lesion and the 12 mm lesion, the most rapid decline in area occurred in the initial interval between 0 cm and 2 cm. In contrast, for the 16 mm and 25 mm lesions, the sharpest reduction in area was observed in the 4 cm to 6 cm interval (Table 7).

Table 7. Quantitative analysis of Area, percentage changes from 0 cm and step changes in Auto ROI according to elevation height

Diameter (mm)	Distance(cm)	Area(cm^2)	Change from 0 cm (%)	Step Change(%)
25	0	409.74	-	-
	2	387.56	-5.4	-5.4
	4	379.35	-7.4	-2.1
	6	352.79	-13.9	-7.0
16	0	269.34	-	-
	2	261.75	-2.8	-2.8
	4	257.96	-4.3	-1.4
	6	227.61	-16.2	-11.8
12	0	220.02	-	-
	2	216.23	-1.7	-1.7
	4	189.67	-14.0	-12.3
	6	155.53	-34.0	-18.0
8	0	163.12	-	-
	2	151.74	-7.0	-7.0
	4	144.15	-11.6	-5.0
	6	136.57	-16.3	-5.3

2.2. Modified ROI Analysis

In the Modified ROI analysis, the area of the smallest lesion (8 mm) decreased by 29.4% at a height of 6 cm compared to the baseline 0 cm, and the 12 mm lesion showed a 23.5% reduction. For the 16 mm and 25 mm lesions, the area decreased by 29.4% and 23.5%, respectively. The analysis of change per distance interval revealed that for the 8 mm smalllesion and the 12 mm lesion, the most rapid decline in area occurred in the initial interval between 0 cm and 2 cm. In contrast, for the 16 mm and 25 mm lesions, the sharpest reduction in area was observed in the 4 cm to 6 cm interval (Table 8).

Table 8. Quantitative analysis of Area, percentage changes from 0 cm and step changes in Modified ROI according to elevation height

Diameter (mm)	Distance(cm)	Area(cm^2)	Change from 0 cm (%)	Step Change(%)
25	0	409.74	-	-
	2	387.56	-5.4	-5.4
	4	379.35	-7.4	-2.1
	6	352.79	-13.9	-7.0
16	0	269.34	-	-
	2	261.75	-2.8	-2.8
	4	257.96	-4.3	-1.4
	6	227.61	-16.2	-11.8
12	0	220.02	-	-
	2	216.23	-1.7	-1.7
	4	189.67	-14.0	-12.3
	6	155.53	-34.0	-18.0
8	0	163.12	-	-
	2	151.74	-7.0	-7.0
	4	144.15	-11.6	-5.0
	6	136.57	-16.3	-5.3

The following graph provides a comparative overview of the percentage change in area relative to the 0 cm baseline for the four lesion sizes, analyzed using the two adaptive ROI methods (Fig. 10).

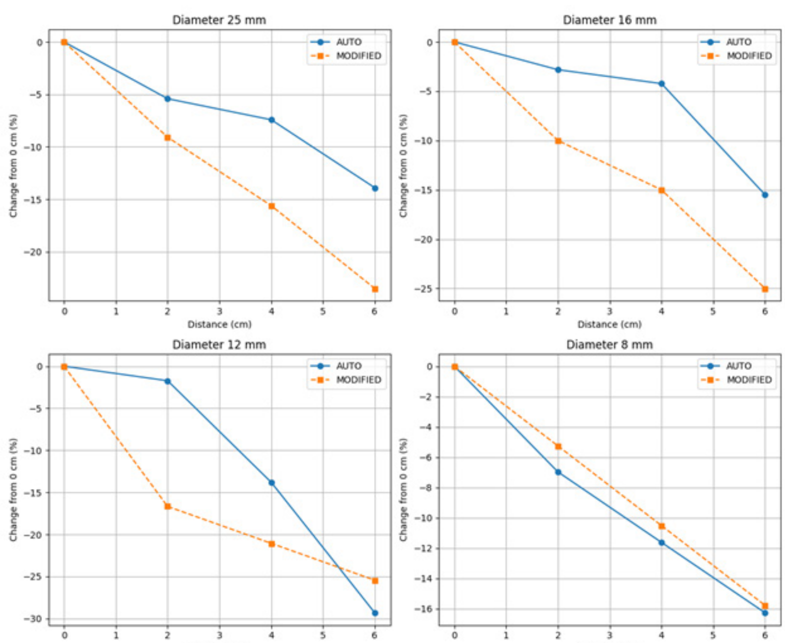

Fig. 10. This figure illustrates the comparison of Area percentage changes from 0 cm analysis using Two different ROI methods: Auto ROI, Modified ROI.

3. FWHM

Compared to the baseline 0 cm, the FWHM at a height of 6 cm increased by 24.9% for the 8 mm lesion and 24.2% for the 12 mm lesion. For the 16 mm and 25 mm lesions, the FWHM increased by 14.7% and 10.1%, respectively. The analysis of change per distance interval revealed that the most significant increases in FWHM for the smaller 8 mm and 12 mm lesions occurred within the initial 0 to 2 cm interval. In contrast, for the larger 16 mm and 25 mm lesions, the sharpest increases were observed in the 4 to 6 cm interval (Table 9).

Table 9. Quantitative analysis of FWHM, percentage changes from 0 cm and step changes in Modified ROI according to elevation height

Diameter (mm)	Distance(cm)	FWHM(mm)	Change from 0 cm (%)	Step Change(%)
25	0	21.46	-	-
	2	22.03	2.7	2.7
	4	22.65	5.5	2.8
	6	23.62	10.1	4.3
16	0	12.91	-	-
	2	13.47	4.3	4.3
	4	14.11	9.3	4.8
	6	14.81	14.7	5.0
12	0	9.78	-	-
	2	10.83	10.7	10.7
	4	11.54	18.0	6.6
	6	12.15	24.2	5.3
8	0	8.51	-	-
	2	9.54	12.1	12.1
	4	10.11	18.8	6.0
	6	10.63	24.9	5.1

The visual analysis of FWHM at each height confirmed that the geometric penumbra (blurring) increases as the distance from the detector grows (Fig. 11). The following graph illustrates the percentage change in FWHM relative to the 0 cm baseline for the four lesion sizes, providing a comprehensive comparison of spatial resolution degradation (Fig. 12).

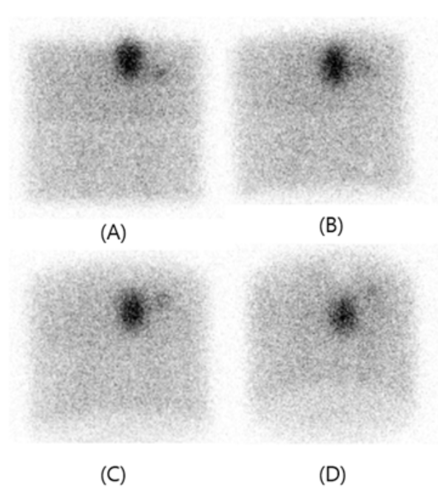

Fig. 11. FWHM analysis of the ACR phantom of 25 ㎜ diameter at varying heights: (A) 0 cm, (B) 2 cm, (C) 4 cm, and (D) 6 cm. An increase in geometric blurring (penumbra) is observed as the distance from the detector increases.

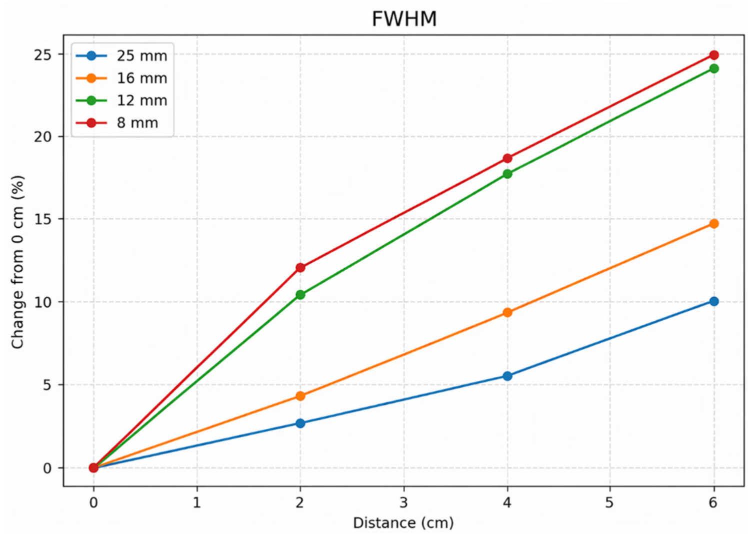

Fig. 12. This figure illustrates the comparison of FWHM percentage changes from 0 cm analysis.

4. Length

At a height of 6 cm compared to the baseline 0 cm, the measured length decreased by 9.4% for the 8 mm lesion and 10.6% for the 12 mm lesion. For the 16 mm and 25 mm lesions, the length reductions were 12.1% and 10.3%, respectively. The interval analysis by distance revealed that the most significant changes in length across all lesion sizes occurred within the 4 cm to 6 cm range (Table 10).

Table 10. Quantitative analysis of Length, percentage changes from 0 cm and step changes in Modified ROI according to elevation height

Diameter (mm)	Distance(cm)	Length(mm)	Change from 0 cm (%)	Step Change(%)
25	0	39.9	-	-
	2	38.6	-3.3	-2.0
	4	37.2	-6.8	-3.6
	6	35.8	-10.3	-3.8
16	0	37.9	-	-
	2	36.5	-3.7	-3.7
	4	35.0	-7.7	-4.1
	6	33.3	-12.1	-4.9
12	0	35.9	-	-
	2	34.7	-3.3	-3.3
	4	33.5	-6.7	-3.5
	6	32.1	-10.6	-4.2
8	0	34.1	-	-
	2	33.4	-2.1	-2.1
	4	32.4	-5.0	-3.0
	6	30.9	-9.4	-4.6

The following graph illustrates the percentage change in length relative to the 0 cm baseline for the four different lesion sizes, providing a clear comparison of the geometric distortion (Fig. 13).

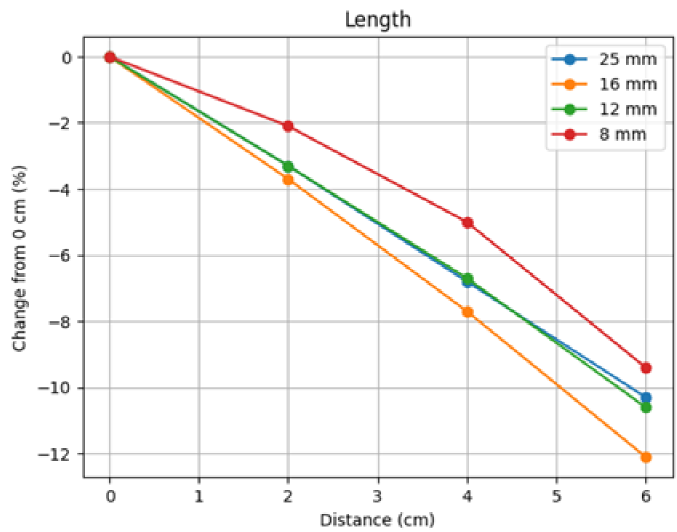

Fig. 13. This figure illustrates the comparison of Length percentage changes from 0 cm analysis

Discussion

The results of this study demonstrate that across all analytical conditions, an increase in height from the 0 cm baseline led to a systematic decrease in total counts, length, and area, while the FWHM exhibited a corresponding upward trend. This rapid increase in FWHM corroborates the fundamental physical principle established by Sorenson et al., which states that geometric resolution degrades as the distance between the collimator and the object increases. These findings prove that smaller lesions are more susceptible to severe signal loss due to the PVE (Partial Volume Effect) and geometric blurring (penumbra) as resolution declines. Consequently, as lesion size approaches the system's FWHM, the "spill-out" effect becomes dominant, accelerating count loss and potentially impairing the detectability of small lesions[6,10,11]. Furthermore, while Fixed ROI analysis showed a relatively uniform decrease of approximately 5–7% across all lesion sizes, Auto ROI analysis revealed significant variability, with the 12mm lesion exhibiting the largest reduction rate of 34.4%. The reason Fixed ROI demonstrated a smaller reduction compared to Auto and Modified ROI is that while Auto ROI excludes pixels with reduced signal intensity due to degraded resolution, Fixed ROI encompasses the blurred peripheral regions, thereby numerically mitigating the decrease. This suggests that although employing a fixed-size ROI in clinical practice may offer advantages in quantitative stability, it is inadequate for comparing actual lesion sizes as it fails to reflect morphological distortion. Additionally, the observation that the measured area decreased despite an increase in FWHM can be attributed to the methodology of ROI definition. In Auto ROI, only pixels exceeding the 80% threshold were included, thereby excluding penumbra regions. Similarly, in Modified ROI, only the high-intensity red range was designated as the ROI. Consequently, the exclusion of blurred peripheral regions, combined with the occurring distortion, led to an underestimation of lesion size as the distance increased. The primary motivation for this study arose from clinical observations where focal uptake in the cranial region of patients undergoing repeated follow-up bone scans appeared to shift in position or disappear between examinations. The image blurring and morphological distortion resulting from a lack of standardized pillow heights necessitate consideration of potential false-negative results, particularly for small lesions. While this study focused on vertical head elevation, lateral head rotation was excluded as a variable. Future investigations exploring distortions caused by head rotation, combined with comparative studies using clinical data, would allow for a more comprehensive analysis. The limitations and methodological considerations of this study are as follows. First, as this was a phantom study using a single 10:1 target-to-background radioactivity ratio, it did not fully replicate clinical complexities such as individual cranial anatomy, patient motion, and scattering effects. Second, the use of planar images from a single dual-head gamma camera and the limited sample size precluded formal statistical analysis. Furthermore, evaluating SNR (Signal to Noise Ratio) and CNR (Contrast to Noise Ratio) was challenging due to confounding variables and ROI reproducibility issues. Third, regarding the examination method, while whole-body scanning may offer broader clinical context, this study utilized spot scanning to closely observe resolution changes in small lesions within the cranium. Spot scanning provides higher count rates and superior statistical precision compared to whole-body scans, which is more consistent with the study's objective of analyzing quantitative distortion patterns. Fourth, the analysis focused on ANT images because pillow height is the primary factor determining the contact proximity between the patient and the detector. Despite the theoretical expectation that resolution should improve as the head approaches the ANT detector, this study sought to quantitatively evaluate the actual morphological distortion and count loss occurring in clinical practice. The focus on ANT images more strongly underscores the necessity for pillow height standardization, as POST images inherently suffer from degradation due to increased distance. Fifth, to minimize inter-observer variability, all analyses were performed by a single technologist. Given the proven reproducibility of Auto ROI, with values remaining constant across five repeated measurements, a single-measurement protocol was consistently applied to all ROI methods to ensure procedural uniformity. Sixth, Styrofoam was selected as the elevation medium to isolate the effects of geometric resolution changes from material-induced attenuation. The linear attenuation coefficient of Styrofoam is significantly lower than that of standard polyurethane foam. Given that both materials, as well as memory foam, have negligible attenuation effects compared to soft tissue (0.150), this choice provided a more objective experimental environment to prove that distance, rather than attenuation, is the primary driver of image distortion. Future research utilizing SPECT to acquire volumetric data is expected to provide more precise analytical insights. As recent studies focus on material compositions that minimize attenuation, motion reduction techniques, and advanced reconstruction algorithms, such integrated approaches are anticipated to significantly enhance diagnostic accuracy in clinical practice.

Conclusion

This study demonstrates that as the degree of elevation the head increases, radioactivity counts decrease significantly due to geometric effects. In small lesions (8 mm and 12 mm cylinders), the most rapid decline in counts was observed within the 0 to 2 cm interval. Conversely, for larger lesions (16 mm and 25 mm cylinders), the reduction in counts became more pronounced after 2 cm, with the magnitude of the decrease further accelerating at distances exceeding 4 cm. Furthermore, the analysis of FWHM revealed that the discrepancy between 0 cm and 6 cm was significantly greater for the 8 mm and 12 mm lesions compared to the larger ones, confirming that smaller lesions are more susceptible to severe distortion. In conclusion, while avoiding the use of a pillow is ideal for maximizing image accuracy, if one must be used for patient comfort, it is recommended to use the lowest possible pillow or headgear, ensuring the height does not exceed 2 cm.

References

1. Ouvrard E, Kaseb A, Poterszman N, Porot C, Somme F, Imperiale A. Nuclear medicine imaging for bone metastases assessment: what else besides bone scintigraphy in the era of personalized medicine?. Front Med. 2024;10:1320574. DOI: https://doi.org/10.3389/fmed.2023.1320574.
2. Kelty NL, Cao Z, Holder LE. Technical considerations for optimal orthopedic imaging. J Nucl Med Technol. 1999;27(1):11-15. DOI: https://doi .org/10.1016/S0001-2998(97)80005-0

3. Seo Y, Aparici CM, Hasegawa BH. Technological Development and Advances in SPECT/CT. Semin Nucl Med. 2008;38(3):177-198. DOI: https://doi.org/10.1053/j.semnuclmed.2008.01.001
4. Ohba M, Kokubo Y, Suzuki K, Kanoto M, Sonoda Y. A Headrest Made of Extruded Polystyrene Reduces the Influence of Attenuation Correction on Human Brain SPECT Images. J Nucl Med Technol. 2023;51(1):44-48.DOI:https://doi.org/10.2967/jnmt.122.264729
5. Ohba M, Kokubo Y, Suzuki K, Kanoto M, Sonoda Y. Influence of a headrest on reconstruction and attenuation correction of human brain SPECT images. J Nucl Med Technol. 2021;49(1):54-57. DOI: https://doi.org/10.2967/jnmt.120.247940
6. Frey EC, Humm JL, Ljungberg M. Accuracy and precision of radioactivity quantification in nuclear medicine images. Semin Nucl Med. 2012;42(3):208-218. DOI: https://doi.org/10.1053/j.semnuclmed.2011.11.003.
7. Meißner T, Cerbone LA, Russo P, Nahm W, Hesser J. Assessment of the axial resolution of a compact gamma camera with coded aperture collimator. EJNMMI Phys. 2024;11:30. DOI: https://doi.org/10.1186/s40658-024-00631-5.
8. El-Kameesy SU, Salama E, Ahmed MS, El-Sersy AR, El-Faramawy N. Improving gamma camera imaging using parallel jagged hole collimator. Radiat Meas. 2023;168:107014. DOI: https://doi.org/10.1016/j.radmeas.2023.107014.
9. Chan C, Liu H, Grobshtein Y, Stacy MR, Sinusas AJ, Liu C. Noise suppressed partial volume correction for cardiac SPECT/CT. Med Phys. 2016;43(9):5051-5062. DOI: https://doi.org/10.1118/1.4961011.
10. Marquis H, Willowson KP, Bailey DL. Partial volume effect in SPECT & PET imaging and impact on radionuclide dosimetry estimates. Asia Ocean J Nucl Med Biol. 2023;11(1):64-75. DOI: https://doi.org/10.22038/AOJNMB.2022.63816.1444
11. Hoffman EJ, Huang SC, Phelps ME. Quantitation in positron emission computed tomography: 1. effect of object size. J Comput Assist Tomogr. 1979;3(3):299-308. DOI: https://doi.org/10.1097/00004728-197906000-00001